Thermomechanical Coupling Model for a Stainless Steel-Clad Plate on Heat Treatment

B. Guan,[1] Y. Zang, F. Yang, X. Y. Yang, and Q. Qin

School of Mechanical Engineering, University of Science and Technology Beijing, Beijing, China

[1] niuben57@163.com

Quick and correct prediction of the internal stress and deformation of stainless steel-clad plates on heat treatment is a problem of specific interest. A thermomechanical coupling model based on the engineering elastic-plastic theory is detailed. The discretization method and difference equations used simultaneously provide effective numerical calculations for the model. The generalized finite element model verifies relevant simplification conditions and efficiency of the numerical calculation logic. Heat treatment experiments of clad plates are also designed and presented, and the ability of the model to predict the stress and deformation behavior of the clad plate in the actual heat treatment process is evaluated. The calculation logic of the model is reasonable, and the prediction error of deformation and internal stress of the plate is ~15%. The model exhibits an extremely high computational efficiency and can meet the requirements of on-line analysis for heat treatment processes.

Keywords: stainless steel-clad plates, heat treatment, thermomechanical coupling model, deformation and internal stress prediction.

Introduction. A stainless clad plate is a kind of laminated composite composed of a stainless steel plate and low-carbon steel or low-alloy steel plate. Such plates have the favorable physical and chemical properties of stainless steel plates, as well as the excellent mechanical properties of the base plate, enabling their use in the nuclear energy, shipbuilding, and oil pipeline industries, among others [1–4]. In order to ensure and improve the material physical and mechanical properties for each layer in the stainless clad plate, heat treatment processes such as controlled cooling and solution treatment are required during the manufacturing of different stainless clad plates [5–7].

The material properties and functional requirements are different for stainless steel and low-carbon steel; the best heat treatment process for each type of layer is different. When designing a heat treatment process for the stainless clad plate, the characteristics of the two different metals must be considered to obtain the best comprehensive service performance. The effects of heat treatment on the material microstructure and mechanical properties of the stainless clad plate have been studied extensively [8–11]. For example, Rao et al. [8] studied the mechanical properties and microstructure of explosively clad HSLA steel with AISI 304L grade under typical quenching and tempering treatment process. Jiang et al. [9] used X-ray diffraction and transmission electron microscopy to examine the microstructure and mechanical properties of Ti-steel explosive-rolling clad plate after different heat treatment processes.

Stainless steel and carbon steel have different thermal conductivities and coefficient of thermal expansion (CET) (among other physical parameters), which can cause asymmetric temperature changes and inconsistent thermal strain during heat treatment. These differences can lead to large deformation with a high macroscopic curvature and high thermal stress levels within the clad plate (Fig. 1), which affects the service performance of the clad plate. Therefore, the heat treatment process significantly affects the microstructure properties of a material, as well as a non-negligible effect on the macroscopic geometrical and mechanical state of the clad plate. In addition to the resulting material microstructure, the thermal stress

Fig. 1. Deformation of stainless clad plate after heat treatment.

level and macroscopic curvature deformation must be fully predicted when designing a heat treatment process for the clad plate. The operation speed of the prediction model must meet the requirements of online heat treatment process analysis. Therefore, an efficient thermo-mechanical coupling model for the clad plate during heat treatment process must be established.

In previous studies, the finite difference method was widely used as an efficient numerical method for online analysis and prediction modeling of the heat treatment process [12–14]. Mukhopadhyay and Sikdar [15] established a one-dimensional online temperature prediction model for the steel plate coiling process with the finite difference method. Saboonchi and Hassanpour [16] simulated the temperature field during the forced cooling process of the hot-rolled coil with the implicit finite difference method, enable them to obtain the temperature distribution in the radial direction of the steel coil. Mansouri et al. [17] studied the effects of heat-retaining conditions on the temperature distribution when the hot-rolled strip passes the transfer table with the finite difference method. Chen et al. [18] proposed an improved finite difference model to predict the temperature changes during ultra-fast cooling more accurately. Due to the symmetrical structure parameters, deformation of traditional plates as caused by thermomechanical coupling effects during heat treatment is not prominent. Therefore, most of these studies focused only on the prediction of a single temperature field during heat treatment; the above models cannot predict the large curvature deformation and internal stress of the clad plate. Some scholars have also used the finite element (FE) method to study the temperature, stress, and phase transition coupling effects of single plates during heat treatment [19–22]. Sun et al. [19] presented a FE model coupled analysis of the thermal and metallurgical behavior of the strip occurring on the run out table cooling. Then, Cho et al. [21] built a three-dimensional FE model to predict the edge wave behavior of hot rolled steel during run out table cooling, which considered the coupling of thermal, metallurgical, and mechanical effects. This kind of multi-field coupling finite element model is very powerful, but the extremely large scale of its calculations makes it unfeasible for analyzing the processing strategy in real time.

In this study, an efficient thermomechanical coupling numerical model was established based on the elastoplastic theory to predict the thermal stress and deformation of stainless clad plates during heat treatment. A finite element model was then built to verify the relevant simplified conditions and the numerical calculation logic rationality of the established thermomechanical coupling numerical model. Heat treatment experiments for the clad plates were designed and conducted, and the ability of the established thermo-mechanical coupling numerical model to predict the stress and deformation behavior was analyzed by comparing the predictions to the actual heat treatment results. The results obtained by the finite element model and the experimental data were compared with the results predicted by the model established in this paper. The latter not only predict accuracy for the stress and deformation behavior of clad plates during heat treatment with high accuracy, but also has a high computational efficiency. Thus, it can realize the online analysis of heat treatment processes.

1. **Establishment of Model**.

1.1. *Model Structure*. By analyzing the physical process of stainless clad plate heat treatment, the change of the temperature field of the clad plate leads to a change in the physical parameters of the material, affecting the mechanical behavior of the plate such as its deformation and internal stress behavior. Hence, the calculation of the mechanical behavior of the clad plate during heat treatment is based on the calculation results of the temperature field. However, the mechanical behavior has little effect on the heat transfer boundary condition and temperature field. Therefore, the heat treatment process of a clad plate is a typical one-way mechanical and thermal coupling problem.

The most efficient way to analyze a one-way coupled physical process is the sequential coupling method. As such, the model in this paper is constructed based on thermomechanical sequential coupling principles, for both the heat transfer model and the mechanical model of the clad plate. In each incremental step, the temperature field of the clad plate is first obtained with the heat transfer model, and then the mechanical parameters and physical parameters related to the material are accordingly fed into the calculation results of the temperature field of the clad plate. Finally, these parameters are input into the mechanical model to solve the deformation and stress field of the clad plate. During solving, the clad plate will be first discretized along the thickness direction. The heat transfer model and the mechanical model will be calculated with the same discretization nodes, which can guarantee effective data transfer between different physical fields and greatly improve the physical field data transfer efficiency. The calculation flow is shown in Fig. 2.
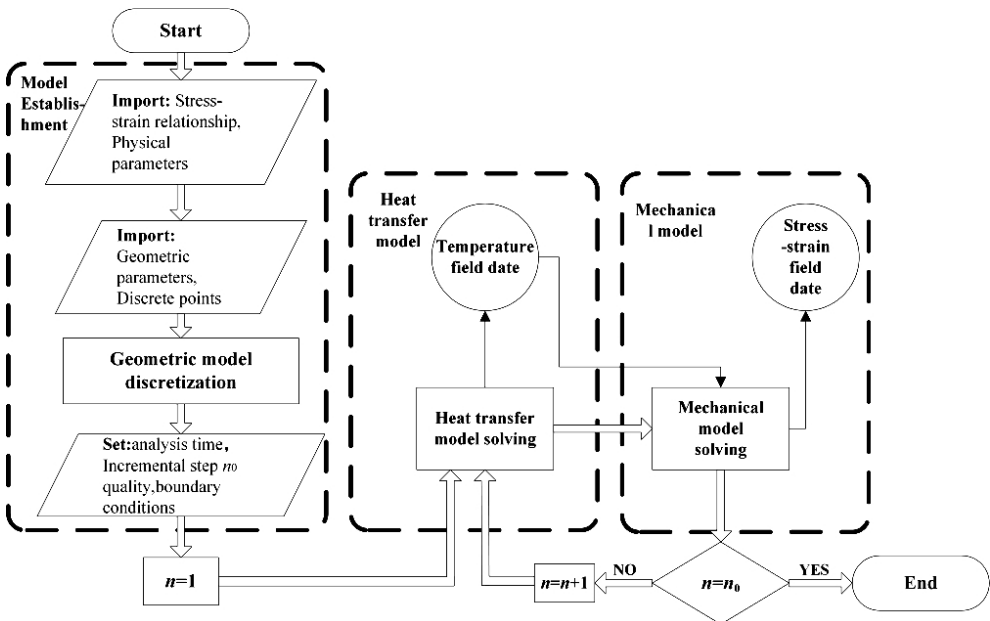

Fig. 2. Calculation flow chart of thermomechanical coupling model.

1.2. *Basic Assumptions of the Model*. Based on the deformation and heat transfer characteristics of heat treatment process for the stainless clad plate heat treatment process, two basic assumptions were made in the present study:

1) Plane section assumption: An arbitrary section of the plate remains flat after deformation. During the heat treatment of the stainless clad plate, the bending deflection of the plate is far smaller than its length, and the height-to-span ratio remains less than 1:5, thus, the plane section assumption is applicable.

2) One-dimensional heat transfer assumption: Compared with a single-material plate, the heat transfer process in a composite metal plate has a key unique feature, namely, the base and cladding materials (which have different thermal physical properties) are laminated along the thickness direction of the plate. This results in obvious property differences in the thermal properties along the thickness direction of the clad plate during heat transfer. This is also the primary cause of the large deformation of the plate after heat treatment. Other conventionally observed deformations in the clad plate are far smaller than the deformation caused by this difference in the thermal properties. Thus, in order to analyze this key feature of the clad plate and to simplify the model, it is reasonable to establish a one-dimensional heat transfer model along the thickness direction of the plate and ignore the special heat transfer conditions at the top and tail regions of the plate.

1.3. ***Heat Transfer Model***.

1.3.1. *Establishment of the Model*. The physical model is shown in Fig. 3a. The total thickness of the clad plate is h, while the thickness of the cladding is h_c, thus, t the thickness of the base is $h - h_c$. Based on the basic principles of heat transfer [23], there is no heat source in the clad plate during the heat treatment process. The one-dimensional thermal conduction differential equation is

$$\begin{cases} \rho_c(z,\tau)c_c(z,\tau)\dfrac{dT(z,\tau)}{d\tau} = \lambda_c(z,\tau)\dfrac{d^2T(z,\tau)}{dz^2} & (h/2 \le z \le h/2 - h_1), \\[4mm] \rho_b(z,\tau)c_b(z,\tau)\dfrac{dT(z,\tau)}{d\tau} = \lambda_b(z,\tau)\dfrac{d^2T(z,\tau)}{dz^2} & (h/2 - h_1 \le z \le -h/2), \end{cases} \tag{1}$$

where $T(z,\tau)$ is the temperature field of the clad plate at any time, τ is the unit time, and $\lambda_c(z,\tau)$ and $\lambda_b(z,\tau)$ are the thermal conductivity of the cladding and the base material, respectively. The density of the cladding and the base material is $\rho_c(z,\tau)$ and $\rho_b(z,\tau)$, respectively, and $c_c(z,\tau)$ and $c_b(z,\tau)$ are the specific heat of the cladding and the base material, respectively.
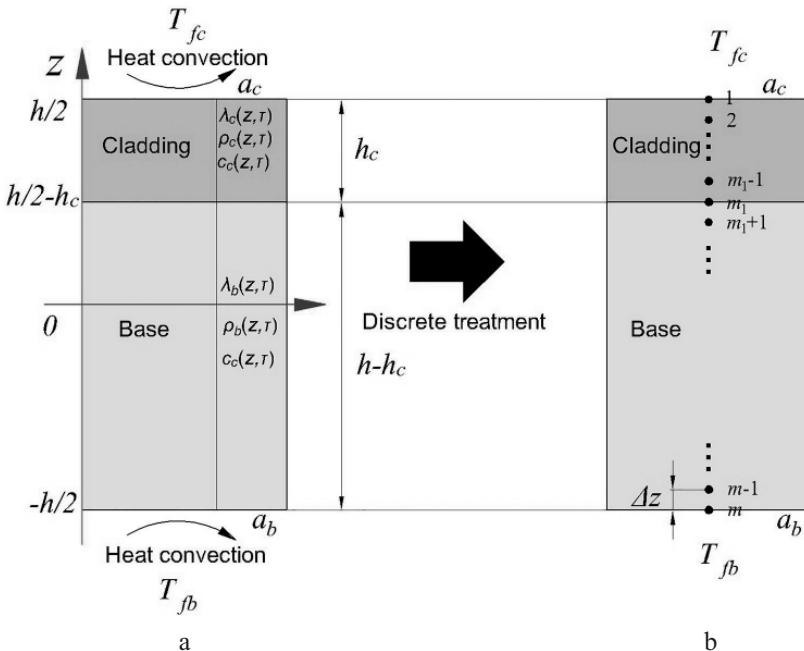

Fig. 3. Schematic diagram of the heat transfer physical (a) and discrete (b) models.

Before the heat treatment process, the metal plate is in a certain soaking state T_0. With that in mind, the initial condition for the differential equations is

$$T(z,\, 0) = T_0 \qquad (0 \leq z \leq h). \qquad (2)$$

During the heat treatment, there is heat transfer between the clad plate surface and the ambient medium, meaning that the convective heat transfer boundary conditions are shown in Eqs. (3) and (4) below. Due to the effective metallurgical bonding at the bimetallic bonding interface of the hot-rolled clad plate, there is no thermal resistance at the bimetallic bonding interface and the temperature is continuously distributed within the clad plate. According to the initial conditions of Eq. (2) and the boundary conditions of Eqs. (3) and (4), the definite solution of the thermal conductivity differential Eq. (1) can be obtained

$$-\lambda_c(z,\tau)\frac{dT(z,\tau)}{dz} = a_c(T_{fc} - T(z,\tau)) \qquad (z = h/2,\, \tau \geq 0), \qquad (3)$$

$$-\lambda_b(z,\tau)\frac{dT(z,\tau)}{dz} = a_b(T_{fb} - T(z,\tau)) \qquad (z = -h/2,\, \tau \geq 0). \qquad (4)$$

1.3.2. Numerical Solution. In order to solve the clad plate heat transfer model established above, the heat transfer model of n time increment steps is numerically solved with the numerical difference method by discretizing the plate along the thickness direction. The specific numerical solution process can be divided into the following two steps.

Discretization of plate: As shown in Fig. 3b, the stainless clad plate is divided into m discretization nodes along the thickness direction. Position coordinates of the discretization nodes are $z_1, \ldots, z_m$, respectively. The cladding is divided into m_1 discretization nodes, and the base is divided into $m - m_1$ discretization nodes. Meanwhile, the base and the cladding share m_1 discretization nodes at the bonding interface to ensure the continuity of the temperature field. Δz is the distance between two discretization nodes, while $\Delta \tau$ is the time length of the increment step. During the numerical calculation process, the temperature $T_1^{(n)}, \ldots, T_m^{(n)}$ of the discretization nodes are used instead the temperature $T^{(n)}(z)$, which is continuously distributed along the thickness direction. The thermophysical parameters $\lambda^{(n)}(z)$, $\rho^{(n)}(z)$, and $c^{(n)}(z)$ of the material are thus replaced by $\lambda_1^{(n)}, \ldots, \lambda_m^{(n)}$, $\rho_1^{(n)}, \ldots, \rho_m^{(n)}$, and $c_1^{(n)}, \ldots, c_m^{(n)}$, respectively.

Establishment of the thermal and boundary difference equations: Based on the coordinates of the discretization nodes, the thermal conduction differential equation of the clad plate and the difference equations of the boundary conditions are established. The thermal conduction differential equation is as follows:

$$\frac{\rho_j^{(n-1)}c_j^{(n-1)}(T_j^{(n)} - T_j^{(n-1)})}{\Delta \tau} = \lambda_j^{(n-1)}\frac{T_{j+1}^{(n)} - T_j^{(n)}}{(\Delta z)^2} - \lambda_{j-1}^{(n-1)}\frac{T_j^{(n)} - T_{j-1}^{(n-1)}}{(\Delta z)^2},$$
$$j = 1, \ldots, m. \qquad (5)$$

The difference equations of heat transfer boundary condition are as follows:

$$\begin{cases} \dfrac{\rho_1^{(n-1)}c_1^{(n-1)}(T_1^{(n)} - T_1^{(n-1)})\Delta z}{\Delta \tau} = \dfrac{\lambda_1^{(n-1)}}{\Delta z}(T_2^{(n)} - T_1^{(n)}) + \alpha_c(T_{fc}^{(n)} - T_2^{(n)}), \\[4mm] \dfrac{\rho_m^{(n-1)}c_m^{(n-1)}(T_m^{(n)} - T_m^{(n-1)})\Delta z}{\Delta \tau} = \dfrac{\lambda_{m-1}^{(n-1)}}{\Delta z}(T_m^{(n)} - T_{m-1}^{(n)}) + \alpha_b(T_{fb}^{(n)} - T_m^{(n)}). \end{cases} \qquad (6)$$

Setting $\dfrac{\rho_j c_j \Delta z}{\Delta \tau} = K_j$ and $\dfrac{\lambda_j}{\Delta z} = A_j$, Eqs. (5) and (6) can be derived into the following difference equations:

$$
\begin{cases}
(\alpha_1 + K_1 + A_1)T_1^{(n)} - A_1 T_2^{(n)} = K_1 T_1^{(n-1)} + \alpha_c T_{fc}^{(n)}, \\
-A_{j-1} T_{j-1}^{(n)} + (K_j + A_j + A_{j-1})T_j^{(n)} - A_j T_{j+1}^{(n)} = K_j T_j^{(n-1)}, \quad j = (2, 3, \ldots, m-1), \quad (7) \\
-A_{m-1} T_{m-1}^{(n)} + (\alpha_{m-1} + K_m + A_{m-1})T_m^{(n)} = K_m T_m^{(n-1)} + \alpha_b T_{fb}^{(n)}.
\end{cases}
$$

By rearranging Eq. (7), a matrix is obtained as follows:

$$
\begin{bmatrix}
\alpha_c + K_1 + A_1 & -A_1 & 0 & 0 & \cdots & 0 \\
-A_1 & K_2 + A_2 + A_1 & -A_2 & 0 & \cdots & 0 \\
0 & -A_2 & K_3 + A_3 + A_2 & -A_1 & \cdots & 0 \\
\vdots & 0 & \cdots & \cdots & \cdots & \vdots \\
0 & \cdots & 0 & -A_{m-2} & K_{m-1} + A_{m-1} + A_{m-2} & -A_{m-1} \\
0 & \cdots & \cdots & 0 & -A_{m-1} & \alpha_b + K_m + A_{m-1}
\end{bmatrix} \times
$$

$$
\times
\begin{bmatrix}
T_1^{(n)} \\
T_2^{(n)} \\
T_3^{(n)} \\
\vdots \\
T_{m-1}^{(n)} \\
T_m^{(n)}
\end{bmatrix}
=
\begin{bmatrix}
K_1 T_1^{(n-1)} + \alpha_1 T_{fc}^{(n)} \\
K_2 T_2^{(n-1)} \\
K_3 T_3^{(n-1)} \\
\vdots \\
K_{m-1} T_{m-1}^{(n-1)} \\
K_m T_m^{(n-1)} + \alpha_{m-1} T_{fb}^{(n)}
\end{bmatrix}.
\tag{8}
$$

This matrix is a three diagonal matrix, which is usually solved numerically using the chase method. By solving Eq. (8), the internal temperature field of the clad plate after $\Delta \tau$ can be obtained according to the result of the upper incremental step and the heat transfer boundary condition. Hence, the heat transfer result can be obtained through iterative calculation using this method.

1.4. *Mechanical Model*.

1.4.1. *Establishment of Model*. As shown in Fig. 4a, the temperature and expansion coefficient both vary along the thickness direction of the clad plate. This produces a nonlinear distributed thermal strain ε_{th} along the thickness direction of the plate, which forms an uncoordinated thermal strain state. Based on the plane section assumption, in order to make the plate section meet the deformation coordination relationship, internal stress must be produced to form a bending deformation with a certain curvature.

The specific establishment process of the mechanical model of this process is as follows. The internal strain and bending curvature accumulated in the plate after the $(n-1)th$ increment step are $\varepsilon^{(n-1)}$ and $C^{(n-1)}$, respectively. In the nth increment step, the expansion coefficient in each position of the plate thickness direction at this time, $\alpha^{(n)}(z)$, can be determined based on the heat transfer model $T^{(n)}(z)$. Based on the temperature field calculation results, $T^{(n)}(z)$ for the nth increment step and $T^{(n-1)}(z)$ for the $(n-1)th$ increment step, the thermal strain $\varepsilon_{th}^{(n)}(z)$ in each position of the plate under free conditions can be obtained as follows:
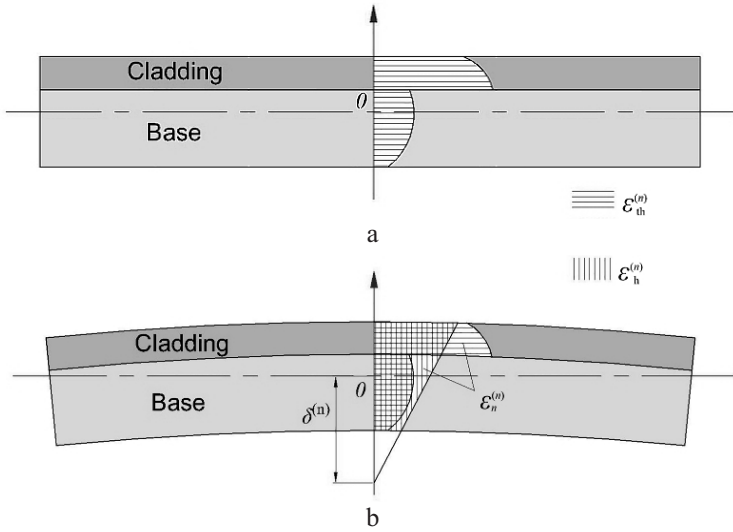
Fig. 4. Schematic diagram of mechanical model: (a) uncoordinated thermal strain $\varepsilon_{th}^{(n)}$; (b) relationship between $\varepsilon_h^{(n)}, \varepsilon_{th}^{(n)}$ and $\varepsilon_{th}^{(n)}, \varepsilon_n^{(n)}$.

$$\varepsilon_{th}^{(n)}(z) = \alpha^{(n)}(z)(T^{(n)}(z) - T^{(n-1)}(z)). \tag{9}$$

However, because of the plane section assumption and deformation coordination relationship, a linear distributed strain $\varepsilon_h^{(n)}(z)$ along the thickness direction of the plate (as shown in Fig. 4b) will be produced in the entire clad plate. The strain is defined as follows:

$$\varepsilon_h^{(n)}(z) = \tan \theta^{(n)} (\delta^{(n)} - z). \tag{10}$$

In the above equation, $\delta^{(n)}$ is the distance between the strain neutral surface of $\varepsilon_h^{(n)}$ and the geometric neutral layer of the plate, $\theta^{(n)}$ is the bending curvature accumulated during the nth increment step of the plate; $\delta^{(n)}$ and $\theta^{(n)}$ are unknowns to be solved. Thus, the actual strain $\varepsilon_n^{(n)}(z)$ produced in the nth increment step is a linear superposition of $\varepsilon_{th}^{(n)}(z)$ and $\varepsilon_h^{(n)}(z)$, namely:

$$\varepsilon_n^{(n)}(z) = \varepsilon_h^{(n)}(z) + \varepsilon_{th}^{(n)}(z). \tag{11}$$

Similarly, according to the linear superposition theory of strain, the total strain $\varepsilon^{(n)}(z)$ on the clad plate accumulated within the nth step is a linear superposition of the total strain $\varepsilon^{(n-1)}$ within the $(n-1)th$ step and the actual strain $\varepsilon_n^{(n)}(z)$ for the nth step, as

$$\varepsilon^{(n)}(z) = \varepsilon_n^{(n)}(z) + \varepsilon^{(n-1)}. \tag{12}$$

According to the stress–strain relationship $\sigma = f(\varepsilon, T)$ for the base and cladding materials, the stress distribution $\sigma^{(n)}(z)$ is obtained using $\varepsilon^{(n)}(z)$ and $T^{(n)}(z)$. $\sigma^{(n)}(z)$ must fulfill the following static force and moment equilibrium equations:

$$\int_{-H/2}^{H/2} \sigma^{(n)}(z)dz = 0, \tag{13}$$

$$\int_{-H/2}^{H/2} \sigma^{(n)}(z)(z - \delta^{(n)})dz = 0. \tag{14}$$

The two unknowns $\delta^{(n)}$ and $\theta^{(n)}$ can be obtained from Eqs. (13) and (14). Furthermore, $\varepsilon^{(n)}(z)$ can be obtained by combining Eqs. (10), (11), and (12), after which the stress distribution $\sigma^{(n)}(z)$ can be obtained. The bending curvature $C^{(n)}$ of the plate at the nth step is given as

$$C^{(n)} = C^{(n-1)} + \theta^{(n)}, \tag{15}$$

$\varepsilon^{(n)}(z)$ and $C^{(n)}$ will be taken as the initial conditions for the $(n+1)$th increment step.

1.4.2. Numerical Simulation. According to the above mechanical analysis model, the mechanical model of the clad plate at the nth time increment step is numerically solved with the same discretization method. The specific numerical solution also can be divided into two steps.

Plate discretization: The clad plate is discretized into $1, \dots, m$ nodes, which are consistent with the discretization node coordinates $z_1, \dots, z_m$ of the heat transfer model. The temperature field calculation results of each node are then transmitted directly to the mechanical model. During the numerical calculation process, the continuously distributed strain $\varepsilon^{(n)}(z)$ and stress $\sigma^{(n)}(z)$ along the thickness direction are replaced by strain $\varepsilon_1^{(n)}, \dots, \varepsilon_m^{(n)}$ and stress $\sigma_1^{(n)}, \dots, \sigma_m^{(n)}$ of the discretization nodes.

Iterative solution of unknown stress and strain of discretization nodes: The temperature field calculation results $T_1^{(n)}, \dots, T_m^{(n)}$ and $T_1^{(n-1)}, \dots, T_m^{(n-1)}$ for step n and step $n-1$ are read into the mechanical model. Using Eq. (9), the thermal strain $\varepsilon_{th1}^{(n)}, \dots, \varepsilon_{thm}^{(n)}$ in free conditions of each discretization node can then be obtained.

The iteration error limits of the static equilibrium equation are set as *eps*1 and *eps*2 for the static moment equilibrium equation, while the number of limit iterations is I. Supposing iteration time $i = 1$, and given a certain initial $\delta_1^{(n)}$ and $\theta_1^{(n)}$, the mechanical model results $\varepsilon_1^{(n-1)}, \dots, \varepsilon_m^{(n-1)}$ of step $n-1$ are read into the mechanical model. The total strain $\varepsilon_{1i}^{(n)}, \dots, \varepsilon_{mi}^{(n)}$ of each node accumulated within the nth increment step is then obtained based on Eqs. (9)–(12).

Through interpolation calculations of the input stress–strain relationship data $\sigma = f(\varepsilon, T)$ of the base and cladding material to the position $(\varepsilon_{1i}^{(n)}, T_1^{(n)}), \dots, (\varepsilon_{mi}^{(n)}, T_m^{(n)})$, the stress $\sigma_{1i}^{(n)}, \dots, \sigma_{mi}^{(n)}$ of each discretization node can be obtained. The static force and moment equilibrium equations (16) of the discretization nodes can be derived from Eqs. (13) and (14). One should check whether $\sigma_{1i}^{(n)}, \dots, \sigma_{mi}^{(n)}$ meet the following criteria using Eqs. (16) or (17):

$$\left| \sum_{j=1}^{m} \sigma_{ji}^{(n)} \right| \le eps1, \tag{16a}$$

$$\left| \sum_{j=1}^{m} \sigma_{ji}^{(n)} (z_j - \delta_i^{(n)}) \right| \le eps2, \tag{16b}$$

$$i = I. \tag{17}$$

If $\sigma_{1i}^{(n)}, \ldots, \sigma_{mi}^{(n)}$ meet any of the above two conditions, $\delta_i^{(n)}$, $\theta_i^{(n)}$, $\varepsilon_{1i}^{(n)}, \ldots, \varepsilon_{mi}^{(n)}$, and $\sigma_{1i}^{(n)}, \ldots, \sigma_{mi}^{(n)}$ are put out as the solution of the unknown stress and strain in the nth increment step. The calculation result $C^{(n-1)}$ of the $(n-1)$th step is then read into the mechanical model. The curvature $C^{(n)}$ after n increment steps is obtained with Eq. (15). If the above conditions are not satisfied, $\delta_i^{(n)}$ and $\theta_i^{(n)}$ need to be reset based on two-dimensional search methods. Meanwhile, setting $i = i+1$, the above operations are performed by iterating until the output conditions are satisfied. The logical frame of the numerical analysis process is shown in Fig. 5.
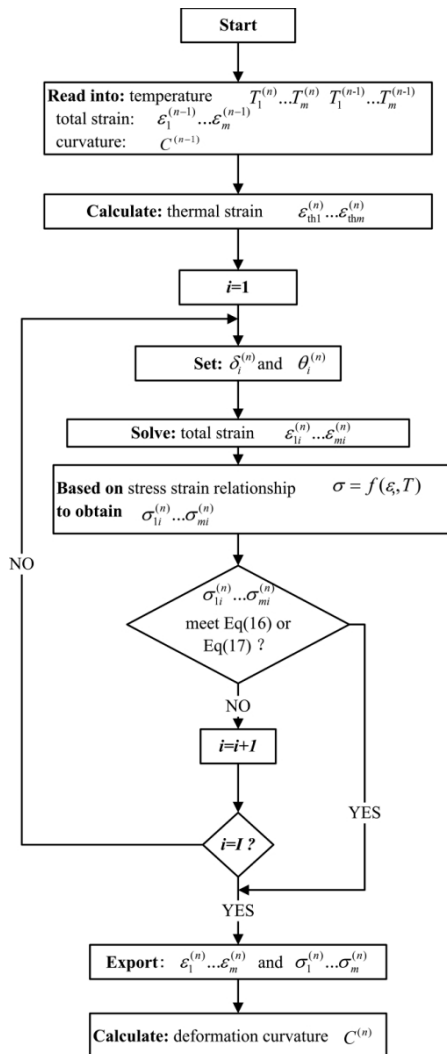

Fig. 5. Logical frame of the mechanical model calculation.

2. **Validity Analysis and Experimental Verification of Model**. In order to validate the simplification and numerical calculation logic of the established model, a two-dimensional thermomechanical coupling finite element model (FEM) is established with ABAQUS to analyze the controlled cooling process. The FEM results are compared to the calculated results of the proposed model. Then, in order to verify the accuracy of the established model in predicting the stress and deformation behavior during heat treatment, a stainless clad plate heat treatment experiment was designed to comparatively analyze the experimental data and prediction results.

2.1. *Mechanical and Physical Properties of Materials*. Accurate mechanical and physical properties are vital to reliable model calculation. Accordingly, the mechanical and physical parameters of the clad plate used in the experimental and numerical simulations were accurately determined using tests or material properties simulation methods.

The base layer is composed of carbon steel Q345R and the clad layer is stainless steel 316L. The chemical compositions of the two materials are shown in Table 1. The expansion coefficients are the most important material parameters affecting the deformation and residual stress of the plate. They are influenced by phase changes, composition etc. Thus, they were precisely measured using a DIL801 thermal dilatometer, and the results are shown in Fig. 6a. The elastic modulus and flow stress are two other important parameters. They describe the stress–strain relationships of the material under elastic and plastic conditions. These two parameters were calculated using the JMatPro software based on the components of two materials, and the result are shown in Fig. 6b–d. Other physical parameters such as the specific heat, conductivity, and Poisson's ratio were also calculated using the JMatPro software.

T a b l e 1

Element Composition of Materials (mass fraction, %)

Steel	C	Si	Mn	P	S	Cr	Ni	Mo	Al	Ti	Fe
Q345R (base)	0.17	0.27	1.40	0.011	0.007	0.023	0.02	< 0.01	< 0.01	< 0.01	Bal.
316L (cladding)	0.017	0.42	1.26	0.031	0.003	16.03	10.03	1.95	< 0.01	< 0.01	Bal.

2.2. *Validity Analysis of Model*. The FE model was established based on a stainless clad plate 500 mm in length and 30 mm in thickness, including 5 mm of cladding (316L) and 25 mm for the base, as shown in Fig. 7. The initial temperature of the plate was set to 900℃ and the cooling process lasted for 30 s. The heat transfer coefficient for both the top and bottom surfaces was 500 W/(m$^2 \cdot$K). The cooling medium temperature was 30℃. CPS4T, the element type of the thermomechanical coupling, was chosen to mesh the plate in the FEM. The cladding is divided into 10 layers, while the base is separated into 20 layers; interfaces between the base and cladding share the same node. The model contains 3000 elements. In the thermomechanical coupling model established here, the total number of discrete nodes m is 180. The cladding is separated into 60 nodes, and the base is discretized into 120 nodes. The time increment step of $\Delta\tau$ is 0.2 s.

Figure 8 shows the results obtained by using the FE model and the proposed model. As can be seen here, the temperature and stress distribution obtained with the proposed model exhibited good agreement with the FEM results, with a maximum difference of < 5%. This shows that the related simplifications and numerical calculation logic of the proposed model are correct and effective. In terms of computational efficiency, the FE model required approximately 30 min of computing time, while the proposed model only
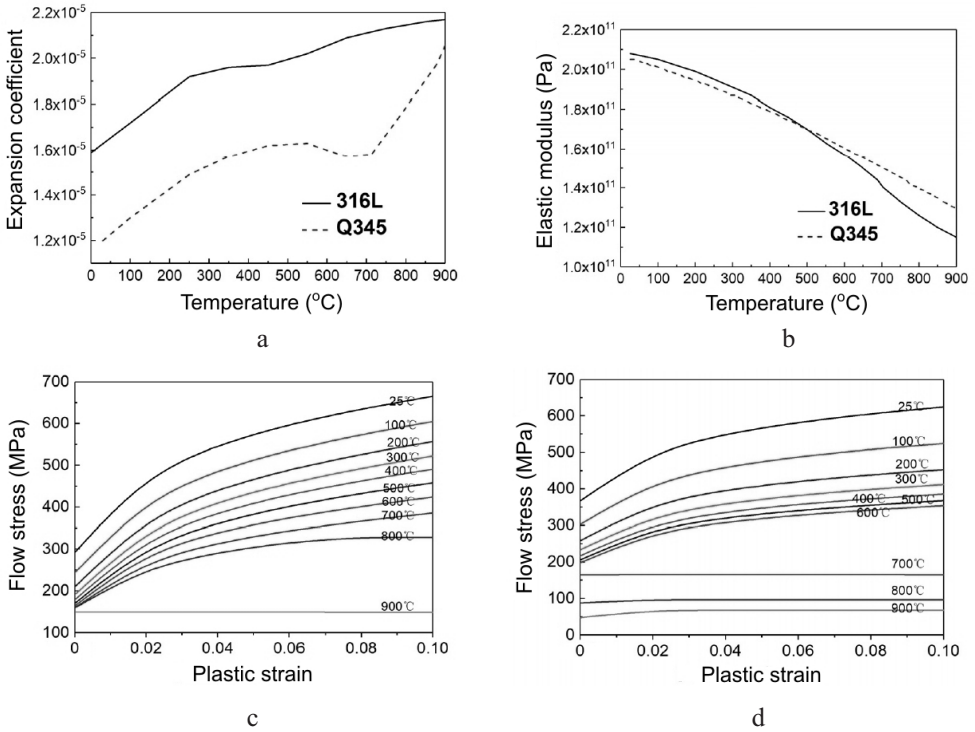
a

b

c

d

Fig. 6. Mechanical and physical properties of materials: temperature dependences for expansion coefficient (a) and elastic modulus (b); stress–strain curves at strain rate 0.001 s^{-1} for 316L (c) and Q345 (d) steels.
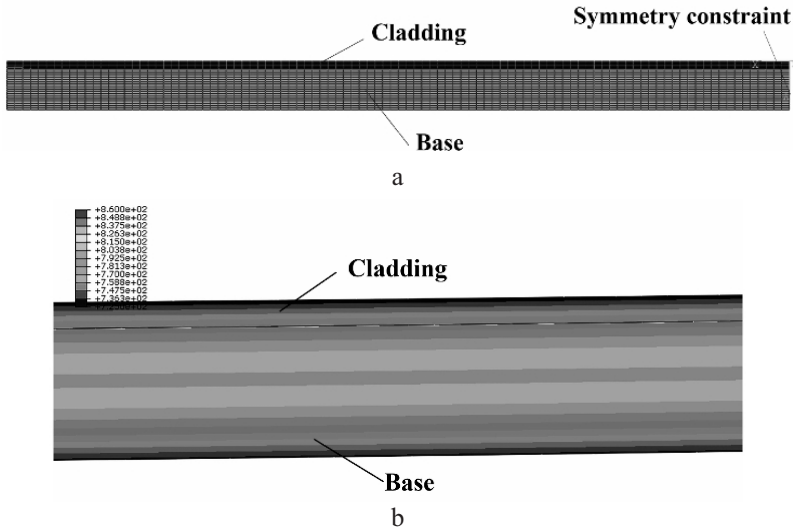

a

b

Fig. 7. Two-dimensional finite element model of thermomechanical coupling: (a) finite element mesh; (b) calculation result of temperature (cooling 20 s).

needed 10 s under the same hardware conditions. Because of its extremely high computational efficiency, the proposed model can rapidly predict stress and deformation behavior, as well as online process strategy analysis, for clad plate heat treatment.
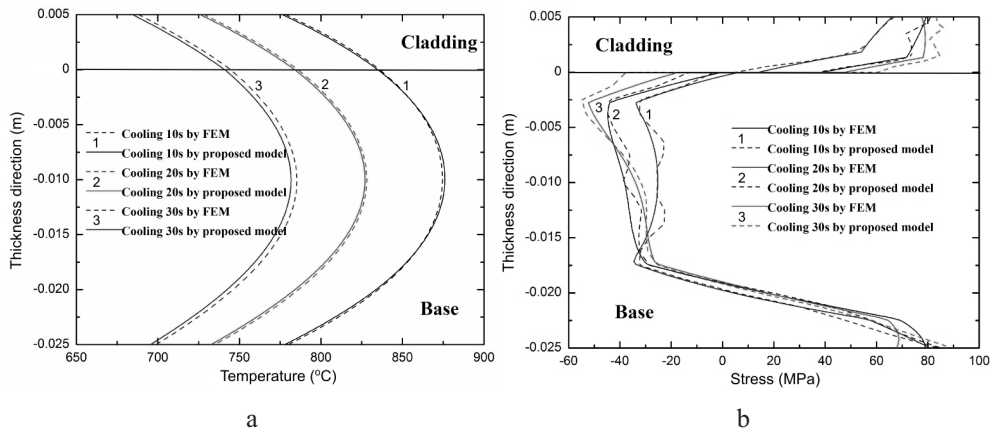
Fig. 8. Comparison of FE and thermomechanical coupling model results: temperature (a) and internal stress (b) distributions in the plate.

2.3. *Experimental Verification of the Model*.

2.3.1. *Experimental Design*. The stainless composite plate used in the experiment is shown in Fig. 9a. The thickness of the base and cladding and their material properties are the same as the FE model (Section 1.1). The concrete dimensions of the test pieces are 1320×350×30 mm (length×width×thickness). Two temperature measuring points are arranged in the inner plate using a thermocouple (Fig. 9b). The 1# point is located at the interface between stainless steel and carbon steel, while the 2# point is located in the center of the clad plate.
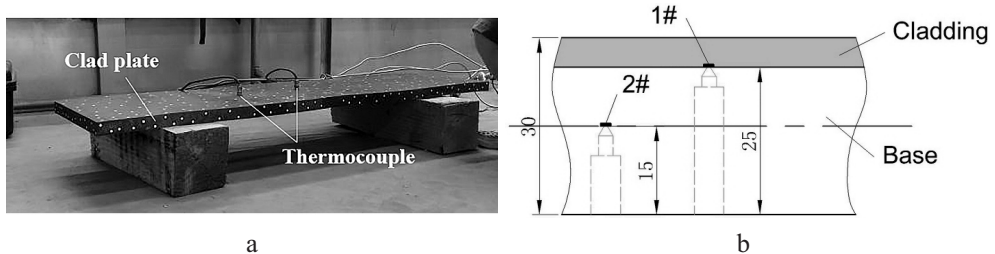

Fig. 9. Experimental plate (a) and location about temperature measuring points (b).

The heat treatment of the plate during the experiments was divided into three steps as shown in Fig. 10a–c. The plate is first put into the heating furnace, and the bonding interface is heated to 950°C and held for 20 min. Next, the plate is removed from the furnace and the stainless steel side of the clad plate undergoes solution treatment with water spraying until the temperature at the bonding interface is reduced to 400°C. Finally, the plate is air cooled to room temperature. After the heat treatment process, the residual stresses of both sides of the plate are determined using a blind-hole method. The deformation curvature is measured by a laser 3D scanning method (Fig. 10d).

2.3.2. *Experimental Results and Analysis*. The temperature data acquired during the heat treatment at the temperature measuring points by the thermocouple are shown in Fig. 11a. The average cooling rate during the spray solution treatment is approximately 3.36 °C/s at the center and 3.98 °C/s at the bonding interface. Because the heating and cooling device used in the heat treatment experiments is relatively simple, it is difficult to control the heat transfer process of the plate surface with the required accuracy and
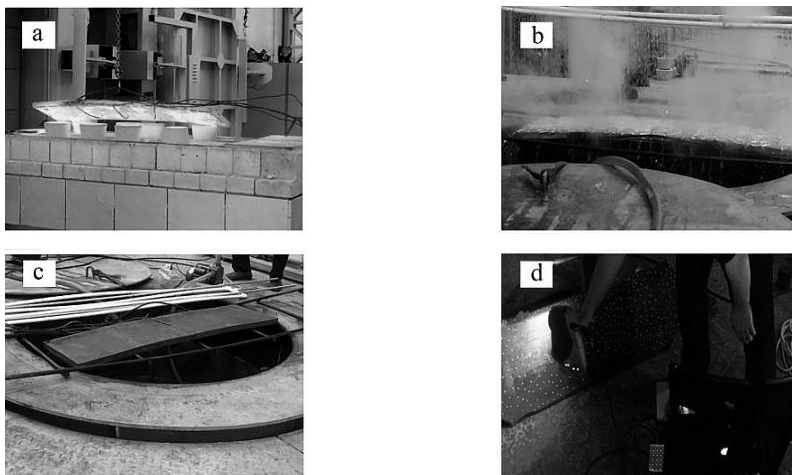
Fig. 10. Clad plate heat treatment experimental process: (a) heating and heat preservation; (b) solution treatment; (c) air cooling; (d) detection.
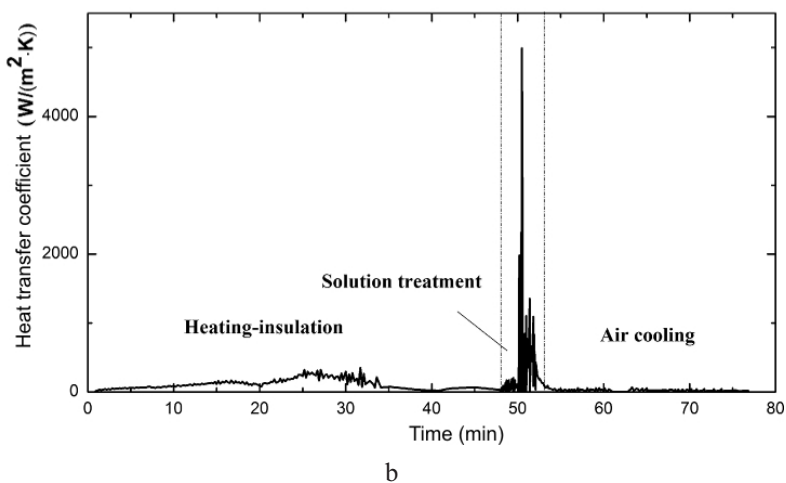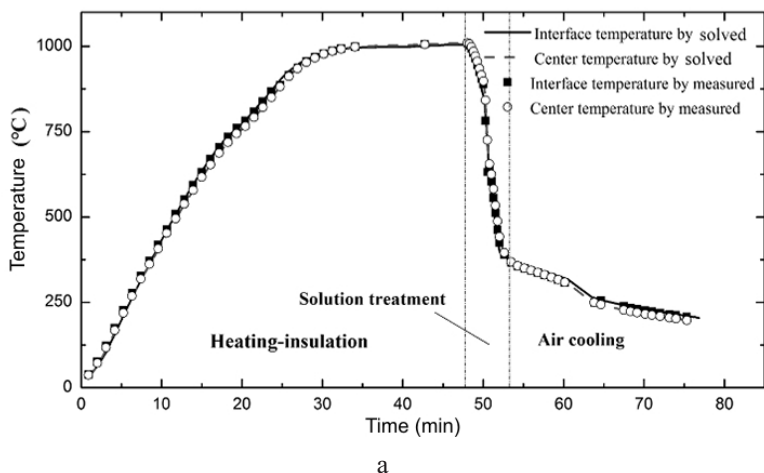

a

b

Fig. 11. Temperature changes with time during experimental heat treatment: (a) experimental process temperature curve; (b) change of surface heat transfer coefficient with time.

stability. Therefore, based on the solution of the inverse thermal conductivity problem, [24] and using the temperature data clad plates measured during experiments, the surface heat transfer coefficient of the clad plate is solved inversely using the heat transfer model established in this article (Fig. 11b). Furthermore, the temperature evolution of each position on the clad plate can be obtained.

The surface heat transfer coefficient obtained by inverse solution is then plugged into the thermomechanical coupling model established in this article, and the residual stress distribution and deformation curvature of the clad plate can be acquired after heat treatment. The residual stresses calculated with the model are compared to the residual stress data of the two surfaces of the clad plate obtained using the blind hole detection method (Fig. 12). According to the calculated results of the model, the center of the plate is in the compressive stress state. However, both surfaces are in the tensile stress state, consistent with the test results. The residual stress calculated value of the base (Q345R) is closer to the detected value with an error of approximately 14.4%; the error is likely to be produced by the detection process. The residual stress error on the cladding surface of 316L between the calculated values and the detection values is relatively larger (27.1%). On the one hand, the error is partly due to the complex heat transfer conditions of the cladding surface. There are significant differences between the ideal calculation model and the actual situation. On the other hand, error arises because the residual stress on the cladding surface exceeds the material yield limit, and the blind hole detection method has a comparatively large error under plastic deformation conditions [25]. The detected results demonstrate that the residual stress on the cladding surface indeed exceeds the material yield limit, agreeing with the calculated results.
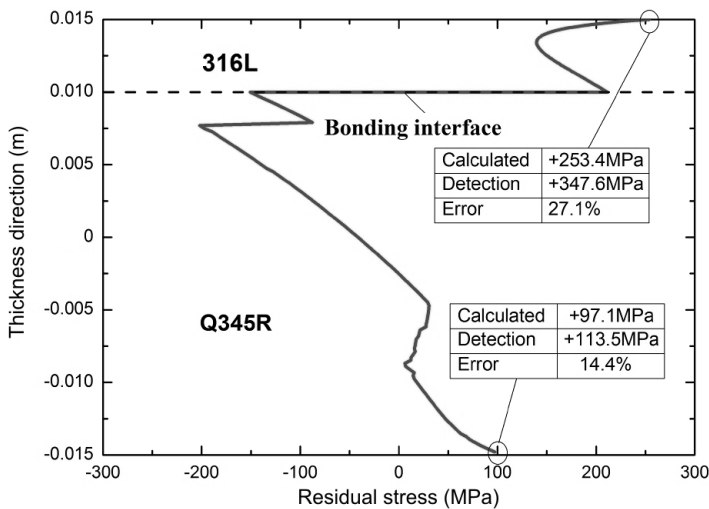

Fig. 12. Residual stress after heat treatment of the plate.

The deformation cloud diagram and the deformation curve of the clad plate acquired by laser 3D scanning are shown in Fig. 13. Clearly, plate deformation occurs in a single one-dimensional curvature state, consistent with the model assumptions. The deformation curvatures of the clad plate obtained through the model calculation and the test data are both shown in Table 2. The results obtained using these two different methods are close to each other, with 15.1% error between them. The measured curves results are larger than the calculated results; the main reason for the error is that the proposed model established in this paper is one-dimensional along the thickness of the plate. This does not consider the special heat transfer conditions at the top and tail regions of the plate. This simplification is

T a b l e 2

The Deformation Curvature of Plate after Heat Treatment

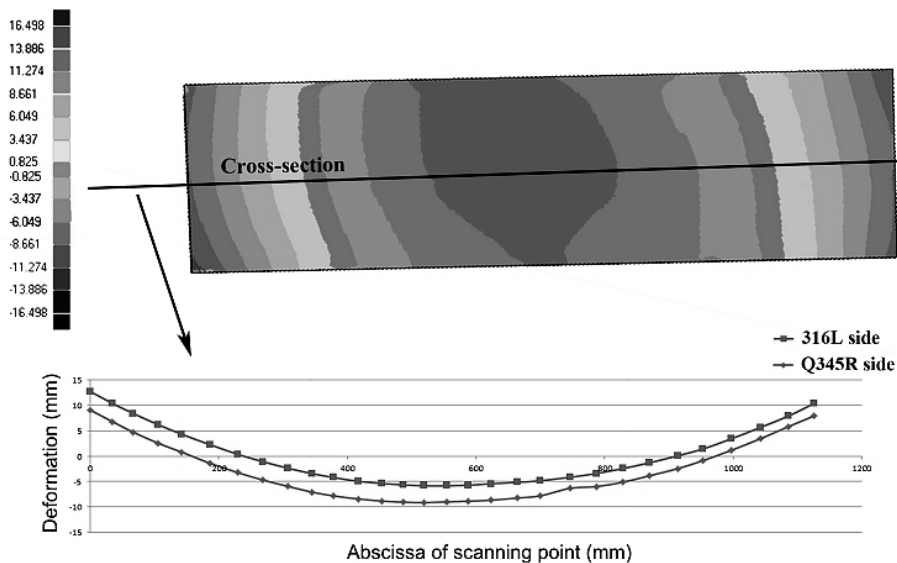| Measured curvature (m^{-1})	Calculated curvature (m^{-1})	Error
0.1199	0.1019	15.01%

Fig. 13. Plate deformation after heat treatment.

reasonable during the actual production process, but the length-thickness ratio of the plate used in this experiment is much greater than those of the plates in actual production environments. As such, the rapid temperature drop at the top and tail of the experimental plate would significantly affect its entire deformation. This can reduce the thermal deformation recovery during the cooling process, thereby increasing the final residual deformation of the plate.

C o n c l u s i o n s

1. Based on engineering elastoplastic theory and heat transfer theory, a thermo-mechanical coupling model aiming at predicting the stress and deformation of a stainless clad plate during heat treatment is established. The discretization method and differential operation are used in combination to implement the efficient numerical calculation of the model.

2. The solving results and computation time of the model established in this paper and the FE model are compared with each other. The difference in solving results between the two models is < 5%. This indicates that the relevant simplification and numerical solution logic of the established model are reasonable. This model has a higher computational efficiency than the general finite element model, enabling it to meet the requirements of the online process strategy analysis for clad plate heat treatment.

3. The model calculation results and experimental data are comparatively analyzed. The model has high prediction accuracy for the stress and deformation behavior of stainless clad plate during actual heat treatment. The prediction error of the deformation curvature and internal stress is approximately 15%.

4. Further studies can improve the structure of the model proposed in this paper. Firstly, some simple microstructural prediction models can be incorporated into this model to comprehensively analyze the micro- and macro-states of the clad plate during the heat treatment. Secondly, based on this model, a finite strip element model can be established to study the shape wave defection problem of clad plates under two-dimensional conditions.

1. Y. Jing, Y. Qin, X. Zang, and Y. Li, "The bonding properties and interfacial morphologies of clad plate prepared by multiple passes hot rolling in a protective atmosphere," *J. Mater. Process. Tech.*, **214**, No. 8, 1686–1695 (2014).

2. L. Li, F. X. Yin, and K. Nagai, "Progress of laminated materials and clad steels production," *Mater. Sci. Forum*, **675–677**, 439–447 (2011).

3. L. Li, K. Nagai, F. Yin, "Progress in cold roll bonding of metals," *Sci. Technol. Adv. Mater.*, **9**, No. 2, 023001 (2008), doi: 10.1088/1468-6996/9/2/023001.

4. M. Yang, X. Zuo, M. Zhao, and J. Wang, "Research Progress of manufacturing technology for stainless steel clad plate," *Hot Work. Technol.*, No. 20, 93–96 (2012).

5. H. Liu, X. Zhang, and L. Li, "Effects of heat treatment on microstructure and properties of hot rolled stainless steel clad plate," *Trans. Mater. Heat Treat.*, **38**, No. 6, 67–70 (2013).

6. G. Xie, Z. Luo, G. Wang, et al., "Interface characteristic and properties of stainless steel/HSLA steel clad plate by vacuum rolling cladding," *Mater. Trans.*, **52**, No. 8, 1709–1712 (2011).

7. I. Hordych, D. Rodman, F. Nürnberger, et al., "Effect of pre-rolling heat treatments on the bond strength of cladded galvanized steels in a cold roll bonding process," *Steel Res. Int.*, **87**, No. 12, 1619–1626 (2016).

8. N. V. Rao, D. S. Sarma, S. Nagarjuna, and G. M. Reddy, "Influence of hot rolling and heat treatment on structure and properties of HSLA steel explosively clad with austenitic stainless steel," *Mater. Sci. Technol.*, **25**, No. 11, 1387–1396 (2009).

9. H. Jiang, X. Yan, J. Liu, and X. Duan, "Effect of heat treatment on microstructure and mechanical property of Ti–steel explosive-rolling clad plate," *T. Nonferr. Metal. Soc.*, **24**, No. 3, 697–704 (2014).

10. M. Yazdani, M. R. Toroghinejad, and S. M. Hashemi, "Effects of heat treatment on interface microstructure and mechanical properties of explosively welded Ck60/St37 plates," *J. Mater. Eng. Perform.*, **25**, No. 12, 5330–5342 (2016).

11. Y. Trykov, L. Gurevich, D. Pronichev, and M. Trunov, "Influence of strain-hardened zones and intermetallic layers of explosion welded and heat treated Al/Cu laminated metal composites on the evolution of thermal conductivity coefficient," *Mater. Sci.*, **20**, No. 3, 267–270 (2014).

12. H. J. Li, L. G. Li, Y. L. Li, and G. D. Wang, "Online monitor and control of cooling temperature on run-out table of hot strip mill," *Steel Res. Int.*, **86**, No. 11, 1225–1233 (2015).

13. Y. Lee, S. Choi, and P. D. Hodgson, "Integrated model for thermo-mechanical controlled process in rod (or bar) rolling," *J. Mater. Process. Tech.*, **125–126**, 678–688 (2002).

14. A. K. Singh and D. Mazumdar, "Comparison of several numerical prediction methods for thermal fields during phase transformation of plain carbon steels," *ISIJ Int.*, **31**, No. 12, 1441–1444 (1991).

15. A. Mukhopadhyay and S. Sikdar, "Implementation of an on-line run-out table model in a hot strip mill," *J. Mater. Process. Tech.*, **169**, No. 2, 164–172 (2005).

16. A. Saboonchi and S. Hassanpour, "Simulation-based prediction of hot-rolled coil forced cooling," *Appl. Therm. Eng.*, **28**, No. 13, 1630–1637 (2008).

17. N. Mansouri, M. Mirhosseini, and A. Saboonchi, "Thermal modeling of strip across the transfer table in the hot rolling process," *Appl. Therm. Eng.*, **38**, 91–104 (2012).

18. X. Chen, G. Wang, Y. Tian, et al., "An on-line finite element temperature field model for plate ultra fast cooling process," *J. Iron Steel Res. Int.*, **21**, No. 5, 481–487 (2014).

19. G. Sun, H. N. Han, J. K. Lee, et al., "A finite element model for the prediction of thermal and metallurgical behavior of strip on run-out-table in hot rolling," *ISIJ Int.*, **42**, No. 4, 392–400 (2002).

20. A. Milenin, R. Kuziak, M. Lech-Grega, et al., "Numerical modeling and experimental identification of residual stresses in hot-rolled strips," *Arch. Civ. Mech. Eng.*, **16**, No. 1, 125–134 (2016).

21. H. H. Cho, Y. G. Cho, D. W. Kim, et al., "Finite element investigation for edge wave prediction in hot rolled steel during run out table cooling," *ISIJ Int.*, **54**, No. 7, 1646–1652 (2014).

22. X. Wang, F. Li, Q. Yang, and A. He, "FEM analysis for residual stress prediction in hot rolled steel strip during the run-out table cooling," *Appl. Math. Model.*, **37**, No. 1, 586–609 (2013).

23. Y. Lu and L. Cheng, *Theory and Analysis of Heat Transfer*, Science Press (1997).

24. Y. Y. Zhang, Z. W. Zhao, Q. Hu, et al., "Establishing and verifying mathematical models of inverse heat conduction problem during aerosol cooling process of the continuous casting," *Comput. Simul.*, **32**, No. 1, 270–273 (2015).

25. A. M. Nawwar, K. McLachlan, and J. Shewchuk, "A modified hole-drilling technique for determining residual stresses in thin plates," *Exp. Mech.*, **16**, No. 6, 226–232 (1976).